Agostini, Thales; Negri, Victor De; Minav, Tatiana; Pietola, Matti

Effect of energy recovery on efficiency in electro-hydrostatic closed system for differential actuator

Published in:
Actuators

DOI:
10.3390/act9010012

Published: 25/02/2020

Document Version
Publisher's PDF, also known as Version of record

Please cite the original version:
Agostini, T., Negri, V. D., Minav, T., & Pietola, M. (2020). Effect of energy recovery on efficiency in electro-hydrostatic closed system for differential actuator. *Actuators*, *9*(1), Article 12. https://doi.org/10.3390/act9010012

actuators

Article

Effect of Energy Recovery on Efficiency in Electro-Hydrostatic Closed System for Differential Actuator

Thales Agostini [1,*], Victor De Negri [1], Tatiana Minav [2,3] and Matti Pietola [3]

1 Department of Mechanical Engineering, LASHIP, Federal University of Santa Catarina, Trindade, Florianópolis 88040-900, Brazil; victor.de.negri@ufsc.br
2 Innovative Hydraulics and Automation Research Group, Tampere University, 33014 Tampere, Finland; tatiana.minav@tuni.fi
3 Department of Mechanical Engineering, School of Engineering, Aalto University, Sahkomiehentie 4, 02150 Espoo, Finland; matti.pietola@aalto.fi
* Correspondence: thalesarb@laship.ufsc.br

Received: 7 January 2020; Accepted: 21 February 2020; Published: 25 February 2020

Abstract: This paper investigates energy efficiency and dynamic behavior through simulation and experiments of a compact electro-hydrostatic actuator system (EHA) consisting of an electric motor, external gear pump/motors, hydraulic accumulator, and differential cylinder. Tests were performed in a stand-alone crane in order to validate the mathematical model. The influence and importance of a good balance between pump/motors displacement and cylinder areas ratios is discussed. The overall efficiency for the performed motion is also compared considering the capability or not of energy recovery. The results obtained demonstrate the significant gain of efficiency when working in the optimal condition and it is compared to the conventional hydraulic system using proportional valves. The proposed system presents the advantages and disadvantages when utilizing components off-the-shelf taking into account the applicability in mobile and industrial stationary machines.

Keywords: electro-hydrostatic actuator (EHA); differential cylinder; efficiency; simulation

1. Introduction

Off-road machines and industrial stationary applications have a huge growth potential with respect to energy savings. Their duty cycle often requires large output power and machine robustness to handle such working loads. In conventional systems, low efficiency is mainly caused by an internal combustion engine (in heavy mobile applications), hydraulic rotational machines, long hoses, and throttling losses of valves to transfer mechanical power to the actuator. In order to improve these drawbacks, a combination of electric and hydraulic technology is an option, considering the high efficiency, reduced noise, and the absence of local emission in electric components [1].

The combination of electric and hydraulic components in a closed circuit defines the concept of electro-hydrostatic actuator systems (EHAs). These systems are a compact and reliable self-contained unit composed of an electric motor, pump/motor, and hydraulic cylinder. EHAs can be driven utilizing three different configurations: Fixed displacement pump and variable speed electrical motor, variable displacement pump and fixed speed motor, and both variable. The latter can provide the highest energy efficiency, however, the cost is higher and it requires more complex control systems in order to achieve maximum efficiency regardless of the hydraulic operation point [2,3].

After all, the concept based on the fixed displacement pump and variable speed electrical motor can offer the lowest manufacturing costs, simplicity, and high efficiency. Though it has a slower dynamic response [2,4]. Several studies have shown the capacity of fixed-displacement pumps being used for distinct applications. An EHA with vane pump is presented in [5] for industrial applications and the virtual prototype represented an effective tool to evaluate the energy consumption in injection molding machines. In [6], an axial-piston pump reaching efficiencies up to 60% during actuation is reported and in [7], an internal gear pump is applied in a high-speed power unit for mobile applications. Aside from the pump working principle, in [8] the authors provided a review of electro-hydraulic technology and presented different circuit configurations for EHA using differential cylinders applications.

Differential cylinders are mostly employed in construction machines due to requirements of output force and installation space. When these actuators are utilized, the inflow and outflow are not balanced, affecting the accuracy in the actuator position, control performance, and energy efficiency.

Flow compensation methods were previously explored, most of them utilizing pilot-operated check-valves [9,10], and shuttle valves [11]. In [12], the influence of hydraulic accumulator to compensate the flow mismatch between cylinder areas and pump displacement on energy efficiency in an open-loop circuit is investigated. Regarding the configurations of pump-controlled systems for differential cylinders, a review and classification is given in [13].

The usage of EHA systems in differential cylinders has been studied extensively, considering the wide possibilities of system configuration and components. This work investigates the performance of a system without implementing the flow compensation method, only relying on the external gear pump/motors available in the market (off-the-shelf), reducing costs.

This paper proposes a circuit layout using two fixed displacement pump/motors driven by one variable speed electrical motor, controlling a differential cylinder in closed circuit operation mode. The system behavior and the energy efficiency are analyzed regarding the flow balance between volumetric displacements of the pump/motors and cylinder areas. The influence of the pressure dependent pump/motor's leakages on balancing the pump/motors and cylinder is discussed and additional hydraulic components are included in order to avoid cavitation and overpressure. The analysis is carried out by simulation using a mathematical model validated through experimental tests. A stand-alone crane setup is utilized in order to test the compact EHA for mobile and stationary applications.

The following section introduces the setup utilized, followed by the mathematical model. After that, Sections 4–6 present results obtained by simulation and experimental data, discussion, and finally conclusions can be found at the end of the paper, respectively.

2. Test Setup

This section describes the structure of the test setup utilized to validate the simulation results. The system was installed in a single-cylinder hydraulic mobile crane as shown in Figure 1. The crane is just for test purposes; no safety regulations or standards were applied for this study case. For the hydraulic part, two external gear motors (which are used as pump/motors) are driven by a permanent magnet synchronous motor. A low-pressure hydraulic accumulator is assembled between the pump/motors to act as a pressurized reservoir, making the system more compact and running in a closed circuit. Three pressure sensors are utilized to collect experimental data to validate the simulation results. In addition, two check-valves are applied to prevent cavitation and two relief valves for safety purposes.

Table 1 presents the parameters of the main components utilized into the test setup. In Figure 2, the system installed in the crane and main components pointed out is shown.

Actuators **2020**, *9*, 12 3 of 16
Actuators **2020**, *9*, 12 3 of 15

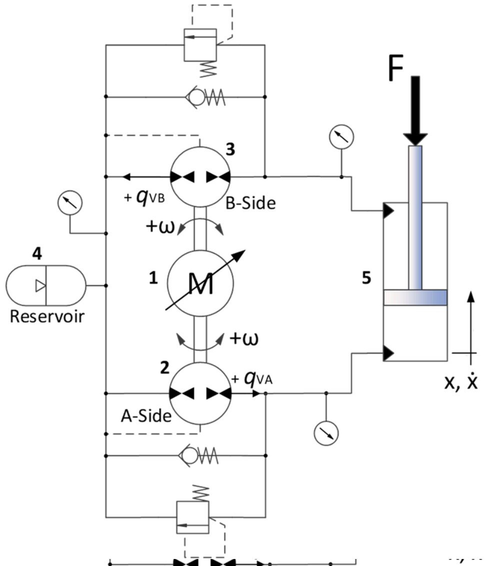

Figure 1. The hydraulic circuit of the test bench.

Table 1. Main parameters of the components in the setup.

No.	Component	Parameters	Value
1	Synchronous Torque Motor	Rated Torque [Nm]	4.5
		Rated Speed [rpm]	2500
2	A-Side ump/Motor	Volumetric Displacement (D_{pm}) [cm^3/rev]	13.03
3	B-Side Pump/Motor	Volumetric Displacement (D_{pm}) [cm^3/rev]	9.35
4	Hydraulic Accumulator	Volume [L]	0.7
5	Cylinder	Dimensions [mm]	60/30 × 400

Figure 1. The hydraulic circuit of the test bench.
Table 1. Main parameters of the components in the setup.

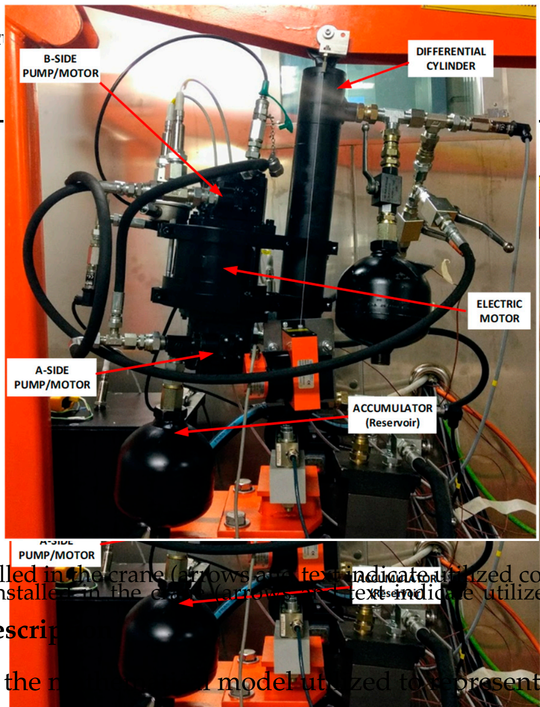

Figure 2. Test setup installed in the crane (arrows and text indicate utilized components for this study).

Figure 2. Test setup installed in the crane (arrows and text indicate utilized components for this study).

3. Mathematical Model Description

This section describes the mathematical model utilized to represent the hydraulic components and the crane load in MATLAB/Simulink. The model considers an ideal source of speed driving two pump/motors. The main parameters utilized in the model are presented later in this section based on experimental validation.

The pump/motor effective volumetric flow rate is expressed by:

$$q_{Vpm} = D_{pm}\omega_{pm} - q_L\Big(\Delta p, \omega_{pm}\Big), \tag{1}$$

where D_{pm} is the volumetric displacement, ω_{pm} is the angular speed, and q_L the sum of internal and external leakages.

The leakages depend on the differential pressure over the pump/motor and its angular speed. They are determined by:

$$q_L = \Big(C_1 + C_2.\big|\omega_{pm}\big|\Big).(\Delta p), \tag{2}$$

where C_1 and C_2 are constant values calculated for each pump/motor based on the manufacturer catalogue information and experimental data.

Three control volumes are considered in the system: The two chambers of the cylinder and the low-pressure volume in the accumulator line. The effective bulk modulus, β_{eff}, represents the total compressibility of the system considering oil, air trapped inside the circuit, and hoses. It is calculated by:

$$\beta_{eff} = \frac{1}{\frac{1}{\beta_H} + \frac{1}{\beta_l} + \left(\frac{V_g}{V_t}\right)\frac{1}{\beta_g}}, \tag{3}$$

where β_H is the bulk modulus of the hoses, β_l is the bulk modulus of the hydraulic fluid, V_g is the volume of air trapped in the system, V_t the total volume, and β_g the bulk modulus of the gas, which is a variable value and considered the instantaneous pressure in the system.

The pressure dynamics of the chambers was modeled utilizing the continuity equation for a control volume, that is:

$$\frac{dp}{dt} = \frac{\beta_{eff}}{V}\left(\sum q_V - \frac{dV}{dt}\right), \tag{4}$$

where dp/dt is the pressure derivative inside the closed volume, V the initial volume of the chamber, and dV/dt the volume variation in time.

The friction force of the cylinder was based on the LuGre model given by:

$$F_{Fr} = \sigma_0 z + \sigma_1\frac{dz}{dt} + \sigma_2 v, \tag{5}$$

$$\frac{dz}{dt} = v - \frac{\sigma_0 z}{g(v)}|v|, \tag{6}$$

$$g(v) = F_C + (F_S + F_C)e^{-(\frac{v}{v_S})^2} \tag{7}$$

where σ_0 is the stiffness of the elastic bristles, σ_1 is the damping coefficient, and σ_2 is the viscous friction coefficient. The z and dz/dt represent the average deflection and deflection rate of the bristles, respectively. $g(v)$ is a positive function and depends, for instance, on material properties, lubrication, and temperature. F_C is the Coulomb friction force, F_S is the static friction force, and v_S is the Stribeck velocity. The friction parameters utilized in the simulation were obtained experimentally previously by [12].

The load force applied in the system is represented by the free body diagram of the crane in Figure 3.

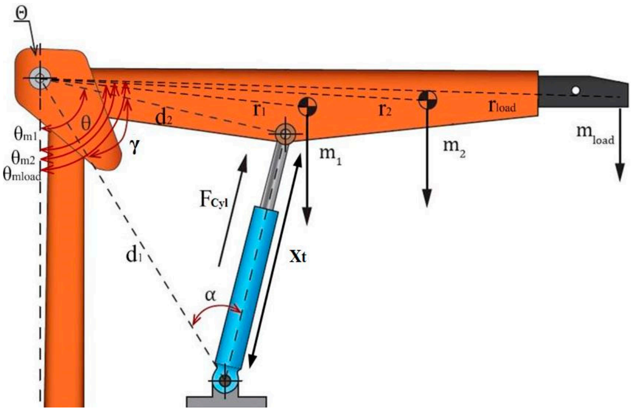

Figure 3. Free body diagram of the crane. (Adapted from [12]).

The load force acts at the extremity of the crane structure generating a torque around the joint Θ, determined by:

$$\sum M_{\Theta} = J\frac{d^2\theta}{dt^2}, \tag{8}$$

where $d^2\theta/dt^2$ is the angular acceleration which can be rewritten decomposing the forces acting in Figure 3 as:

$$\frac{d^2\theta}{dt^2} = \left(\frac{1}{J}\right)\left[\left(-m_1.r_1.sin(\theta_{m1}) - m_2.r_2.sin(\theta_{m2}) - m_{load}.r_{load}.sin(\theta_{mload})\right)g + F_{Cyl}.sin(\alpha).d_1\right], \tag{9}$$

where m_1 and m_2 are the masses of the segments the crane is composed of, r_1 and r_2 are the distance between the centre of mass of each segment and the joint, θ_{m1} and θ_{m2} are the angle between the center of mass and the reference perpendicular axis, and g is the gravitational constant. Payload is attached to the crane with a chain. For simplification, the load is considered at the point the chain is attached to the movable part, such that m_{load} considers the mass of the load, chain, and the hook. F_{Cyl} is the net hydraulic force, α is the angle between the cylinder and the joint, and d_1 the distance between the cylinder base and the joint.

The angles γ, θ_{m1}, θ_{m2}, and θ_{mload} shown in Figure 3 can all be determined in the function of θ by their initial values measured when the cylinder is fully retracted plus the variation of θ:

$$\gamma = \gamma_0 + \frac{d\theta}{dt}, \tag{10}$$

$$\theta_{m1} = \theta_{m10} + \frac{d\theta}{dt}, \tag{11}$$

$$\theta_{m2} = \theta_{m20} + \frac{d\theta}{dt}, \tag{12}$$

$$\theta_{mload} = \theta_{mload0} + \frac{d\theta}{dt}, \tag{13}$$

and angle α is found using the sine rule given by:

$$sin(\alpha) = \frac{d_2}{x_t}sin(\gamma), \tag{14}$$

where d_2 is the distance of the upper fastening point of the cylinder and the joint. x_t is the body length of the cylinder when fully retracted plus the stroke displacement. To obtain x_t the cosine rule is utilized, resulting in:

$$x_t = \sqrt{{d_1}^2 + {d_2}^2 - 2d_1d_2cos(\gamma)}. \tag{15}$$

Deriving Equation (15) in function of time t, the velocity of the cylinder can be expressed by:

$$\frac{dx}{dt} = \frac{d_1 d_2 \frac{d\gamma}{dt} \sin(\gamma)}{\sqrt{d_1^2 + d_2^2 - 2 d_1 d_2 \cos(\gamma)}} \tag{16}$$

Check valves for anti-cavitation purposes were modeled as an orifice allowing volumetric flow from the reservoir to the cylinder chambers when the pressure difference over the valves is 2.5 bar. The pressure relief valves were also modeled as an orifice that allows volumetric flow when the chamber pressure reaches the cracking pressure. The influence of the valve dynamic was not investigated.

The following sections present the experiment results and the model validation, as well as the energy analysis.

4. Model Validation

Experiments were carried out to evaluate the system performance and validate the mathematical model. A constant load force of approximately 392 N (40 kg) was applied on the crane and a rotational frequency of the electric motor was used as an open-loop reference input as shown in Figure 4. Both disturbance and reference inputs were used as model inputs for simulation. The cylinder position and chamber pressures, as well as the accumulator line pressure, were recorded and compared with the simulation results. The system parameters are those presented previously in Table 1 complemented with Table 2. The closed circuit is shown as highly sensitive to the parameter values, mainly regarding pump/motor leakage coefficients, volumetric displacement, cylinder friction coefficients, and check-valve opening pressure.

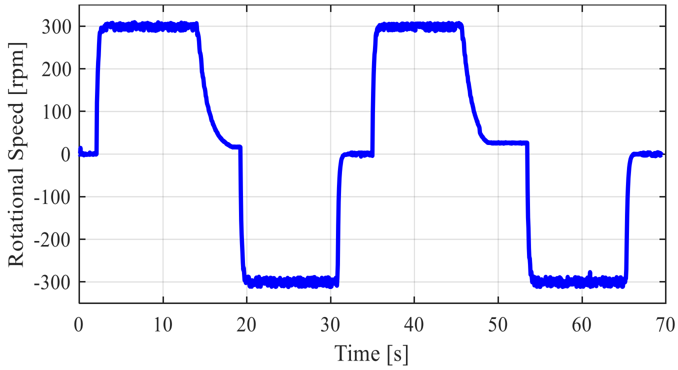

Figure 4. Electric motor rotational speed measured by the encoder.

Table 2. Pump/motor parameters.

Parameter	Values	Parameter	Values
C_{1_A} [m^3/s/Pa]	1.604×10^{-12}	d_1 [m]	0.983
C_{2_A} [m^3/Pa]	2.559×10^{-14}	d_2 [m]	0.647
C_{1_B} [m^3/s/Pa]	1.4×10^{-11}	m_1 [kg]	25.11
C_{2_B} [m^3/Pa]	2.515×10^{-13}	m_2 [kg]	21.40
σ_0 [N/m]	300000	m_{load} [kg]	40
σ_1 [Ns/m]	547.72	r_1 [m]	0.693
σ_2 [Ns/m]	10000	r_2 [m]	0.977
F_c [N]	240.61	r_{load} [m]	1.674
F_s [N]	300	θ_{m10} [rad]	0.1169
v_s [m/s]	0.0005	θ_{m20} [rad]	0.1572
β_H (Pa)	7×10^8	θ_{mload} (rad)	0.1775
β_L (Pa)	1.4×10^9		

Experimental and simulation responses are presented in Figures 5–8. As can be seen, the mathematical model represents very well the cylinder position through all cycle trajectories with a maximum error of 1 mm on the top and 4–5 mm on the bottom. The experimental pressure behavior in the cylinder chambers A and B were reproduced by simulation along with the accumulator line pressure, shown in Figure 8, corroborating the ability of the model to describe the crane behavior.

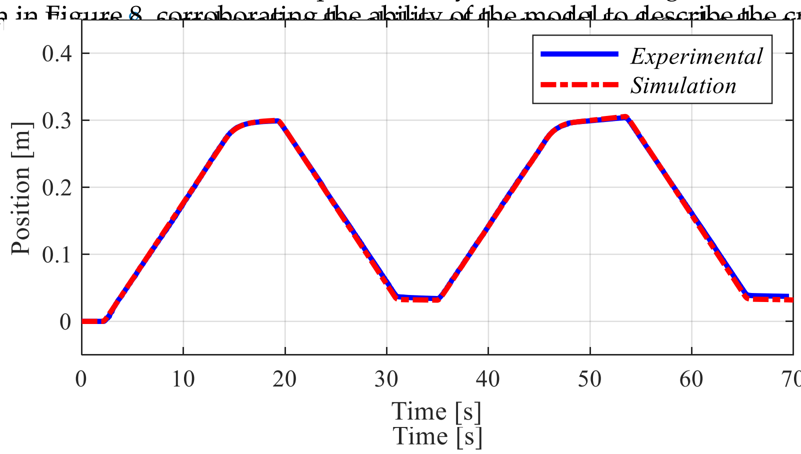

Figure 5. Cylinder position.

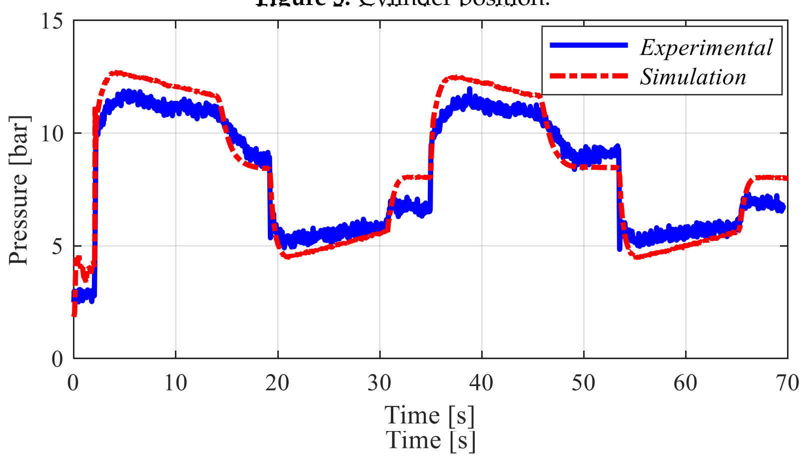

Figure 6. Piston head side chamber pressure.

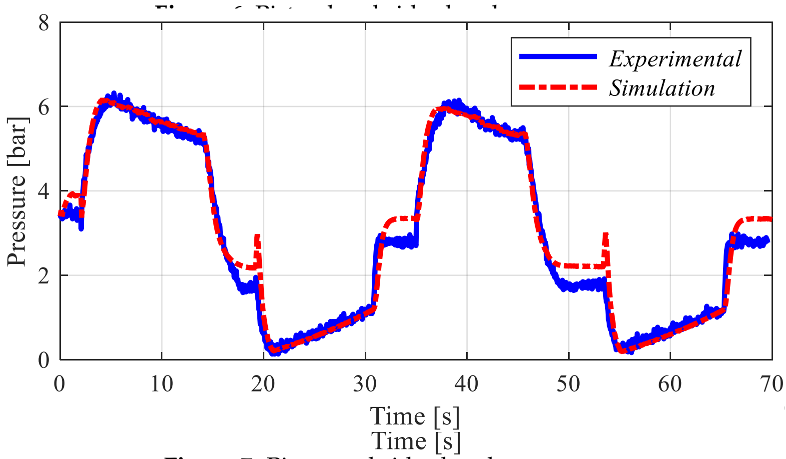

Figure 7. Piston rod side chamber pressure.

Actuators **2020**, *9*, 12 8 of 15

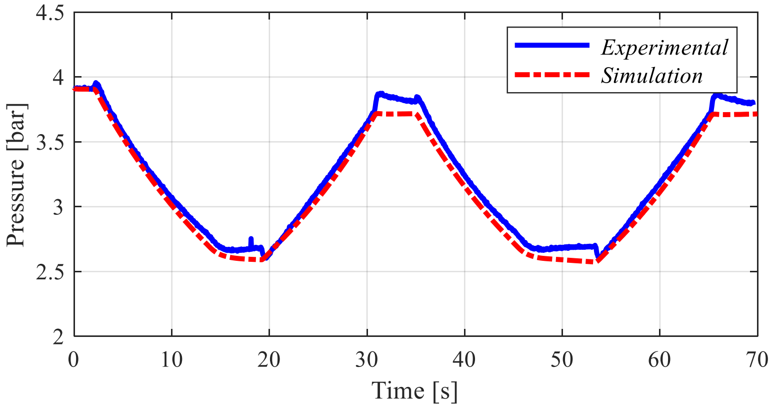

Figure 8. Accumulator line pressure.

5. Results and Discussion

5.1. Energy Analysis

Using the validated model presented above, the system is now analyzed in terms of consumed and delivered power, as well as energy efficiency. The influence of ratio between pump/motor displacements and cylinder areas is also discussed.

The torque T required by both pump/motors is calculated by:

$$T = \Delta p.D_{pm}/\eta_{mech}, \quad (17)$$

and the power at the electric motor shaft is given by:

$$P_{em} = T.\omega, \quad (18)$$

where mechanical efficiency, η_{mech}, is based on the catalogue data.

The useful cylinder mechanical power is calculated by:

$$P_{Cyl} = F_{Cyl}\frac{dx}{dt}, \quad (19)$$

where F_{Cyl} is the net force exerted by the cylinder and x is the position.

The electric motor and cylinder powers along the cycle are presented in Figure 9. The time intervals where the power values are positive represent the lifting motion and the negative values represent the lowering motion. In order to estimate the energy and efficiency all over the cycle, the input and output powers are defined according to the flow power direction. In other words, when the actuator is advancing, the input power is considered on the electric motor shaft and the output power on the cylinder piston. In the opposite motion direction, the input power is that resulting from the load potential energy and the output power is on the motor shaft.

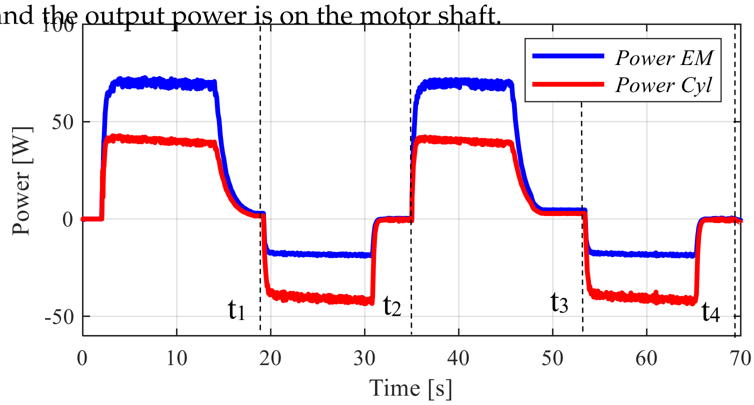

Figure 9. Instantaneous power during the cycle.

intervals where the power values are positive represent the lifting motion and the negative values represent the lowering motion. In order to estimate the energy and efficiency all over the cycle, the input and output powers are defined according to the flow power direction. In other words, when the actuator is advancing, the input power is considered on the electric motor shaft and the output power on the cylinder piston. In the opposite motion direction, the input power is that resulting from the load potential energy and the output power is on the motor shaft.

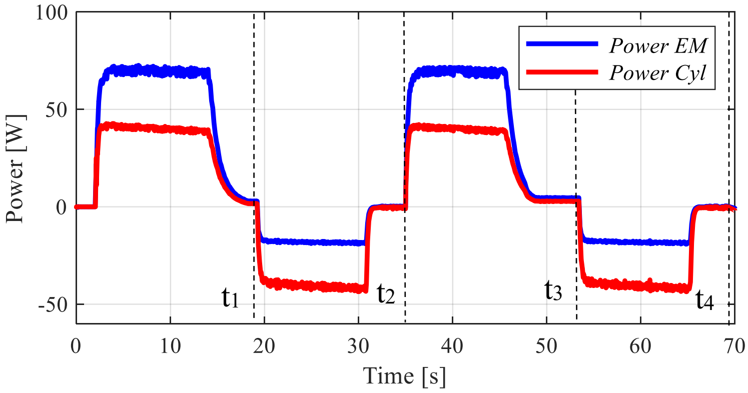

Figure 9. Instantaneous power during the cycle.

The input and output energies are determined by integrating the powers in each motion and sum given by:

$$E_{input} = \int_0^{t1} T.\omega.dt + \int_{t1}^{t2} F_{Cyl}.|\dot{x}|.dt + \int_{t2}^{t3} T.\omega.dt + \int_{t3}^{t4} F_{Cyl}.|\dot{x}|.dt, \quad (19)$$

$$E_{input} = \int_0^{t1} T.\omega.dt + \int_{t1}^{t2} F_{Cyl}.|\dot{x}|.dt + \int_{t2}^{t3} T.\omega.dt + \int_{t3}^{t4} F_{Cyl}.|\dot{x}|.dt, \quad (20)$$

and

$$E_{output} = \int_0^{t1} F_{Cyl}.\dot{x}.dt + \int_{t1}^{t2} T.|\omega|.dt + \int_{t2}^{t3} F_{Cyl}.\dot{x}.dt + \int_{t3}^{t4} T.|\omega|.dt. \quad (20)$$

$$E_{output} = \int_0^{t1} F_{Cyl}.\dot{x}.dt + \int_{t1}^{t2} T.|\omega|.dt + \int_{t2}^{t3} F_{Cyl}.\dot{x}.dt + \int_{t3}^{t4} T.|\omega|.dt. \quad (21)$$

where the time instants are shown in Figure 9.

The energy analysis can be done in two different approaches. First, considering that the energy available in the electric motor shaft when lowering the crane can be sent back to the grid (or battery pack), recovering energy. In this case, the overall efficiency is determined considering all parts involved in Equation (21).

The other approach is not considering the capacity of energy recovery, working similarly to the conventional meter-out flow control system and wasting the stored potential energy. The energy in the electric motor shaft is just dissipated and, consequently, there is not an opposite torque. In this case, the torque (T) dependent terms in Equation (20) are neglected.

Energy values with and without energy recovery can be seen in Figure 10.

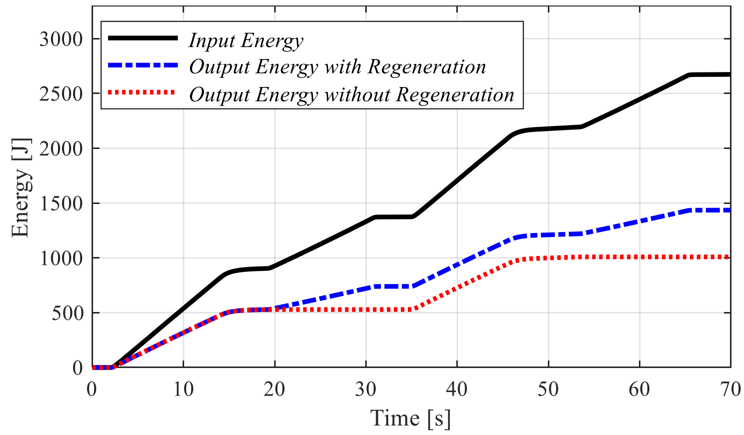

Figure 10. Overall energy during the cycle considering energy recovery (blue line) and without recovery (red line).

In Figure 10, the black line corresponds to the input energy involved to perform the whole motion present, the red line consists of the total mechanical energy from the cylinder motion, and the blue presents the amount of mechanical energy of the cylinder plus the amount for energy that is captured by the electric motor during the cylinder retraction.

The total efficiency when the system is able to recover energy resulted in approximately 54%, while the system without energy recovery was around 38%. These values are only taken into account the hydraulic component losses, not considering the energy conversion at the electric motor.

5.2. Influence of the Volumetric Displcacemnt Ratios

The total efficiency when the system is able to recover energy resulted in approximately 54%, while the system without energy recovery was around 38%. These values are only taken into account the hydraulic component losses, not considering the energy conversion at the electric motor.

5.2. Influence of the Volumetric Displcacemnt Ratios

It is important to notice that the leakages of both pump/motors have a significant influence on the system performance, especially when operating in higher rotational frequencies as shown in Equation (2). When the cylinder is advancing, the flow suction of the pump/motor on the rod side chamber (B-Side) is lower than the resulting from the cylinder displacement creating a counter pressure in the actuator chamber B (see Figure 7). The faster the cylinder moves, the higher the pressure is, limiting the crane operation range. In this system condition, when rotational frequencies are higher than 550 rpm, the pressure relief valve opens (30 bar). As the pressure in chamber B increases, the pressure in chamber An increases as well, resulting in a higher net torque in the pump/motor shaft.

To improve the energy efficiency, two possible approaches are proposed. The first one is utilizing the pressure relief valve in order to avoid the counter pressure caused by the unbalance volumetric displacements of pump/motors compared to the area ratio of the actuator. A low cracking pressure of the valve can significantly improve the efficiency and allow operation with high speed. The second one is to match the effective volumetric flow of the pump/motors with the effective inflow and outflow of the actuator. A thorough analysis needs to be carried out regarding the real volumetric displacement and the real leakage curve, in a function of differential pressure and rotational frequency in each pump/motor. This would provide the range conditions the system could operate to maximize its efficiency. Considering this, the second approach is desirable, once it can overcome the relief valve losses.

To investigate the influence and sensitivity of the correct ratio between areas and displacements, different dynamic behaviors were analyzed by adjusting the B-Side pump/motor displacement. The analyzed displacement ratios vary from the experimental setup value (0.717) to the assumed optimal condition based on the cylinder area ratio (0.75). The simulation conditions considered a load mass of 200 kg and a maximum rotational frequency of 600 rpm. The input rotational speed and the cylinder position are shown in Figures 11 and 12, respectively. The pressure levels in the cylinder chamber are illustrated in Figures 13 and 14 for four displacement ratios between the pump/motors. Figure 15 presents the corresponding accumulator line pressure.

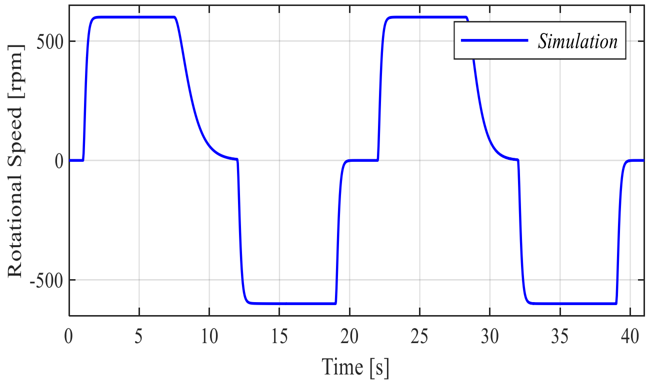

Figure 11. Pump/motor rotational speed.

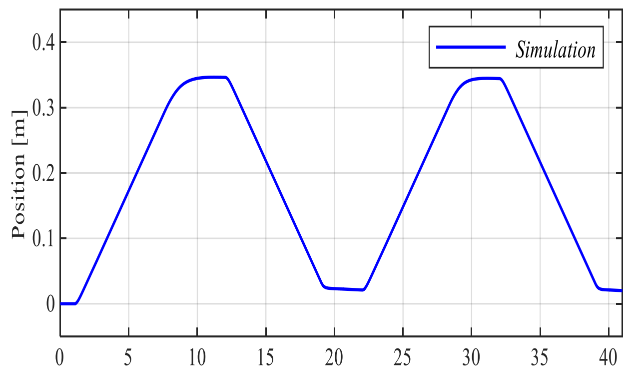

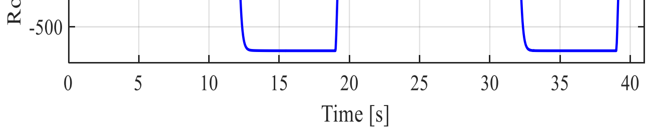

Figure 11. Pump/motor rotational speed.

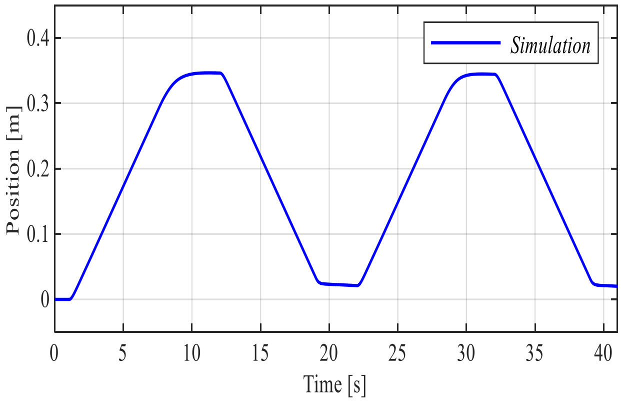

Figure 12. Cylinder position (600 rpm).

Figure 12. Cylinder position (600 rpm).

As shown in Figure 13, the pressures have a sudden increase during the lifting motion when the displacement ratio is not near the optimal value. The pressures in Figure 14 are limited by the relief valves on the rod side and a lower cracking pressure could lead to higher efficiencies due to smaller counter-pressure generated. This high sensitivity on the ratio unbalance (0.01) supports the idea that each operation condition has an optimal condition of ratios due to the pump leakages varying with rotational frequency and the pressure over the pumps. In order to obtain a better condition as close as possible, the 0.75 ratio should be used for both pumps and cylinder areas. Utilizing fixed-displacement pump/motors, with volumetric flow depending on the pressure and rotational speed, it is impossible to achieve its maximum potential without auxiliary valves. Another fact to be considered in this system is the load force direction, in this case a static compression load is reducing the complexity to work with this system configuration so the valves can passively work. In other words, the absence of change of load direction implies no need of piloted valves.

As shown in Figure 13, the pressures have a sudden increase during the lifting motion when the displacement ratio is not near the optimal value. The pressures in Figure 14 are limited by the pressure relief valves on the rod side and a lower cracking pressure could lead to higher efficiencies due to smaller counter-pressure generated. This high sensitivity on the ratio unbalance (0.01) supports the idea that each operation condition has an optimal condition of ratios due to the pump leakages varying with rotational frequency and the pressure over the pumps. In order to obtain a better condition as close as possible, the 0.75 ratio should be used for both pumps and cylinder areas. Utilizing fixed-displacement pump/motors, with volumetric flow depending on the pressure and rotational speed, it is impossible to achieve its maximum potential without auxiliary valves. Another fact to be considered in this system is the load force direction, in this case a static compression load is reducing the complexity to work with this system configuration so the valves can passively work. In other words, the absence of change of load direction implies no need of piloted valves.

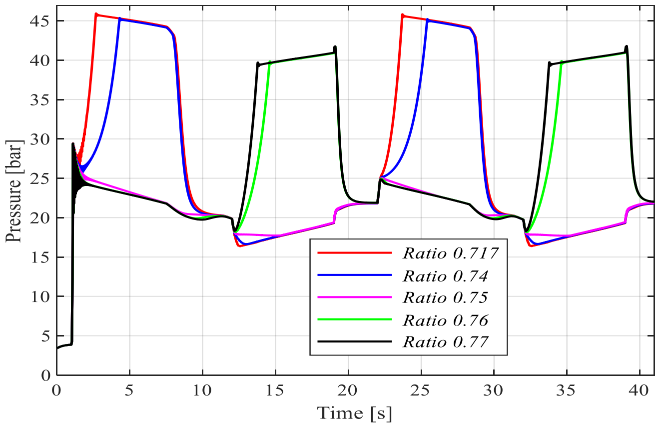

Figure 13. Pressure in the piston head chamber for different displacement ratios. Cracking pressure = 30 bar.

Figure 13. Pressure in the piston head chamber for different displacement ratios. Cracking pressure = 30 bar.

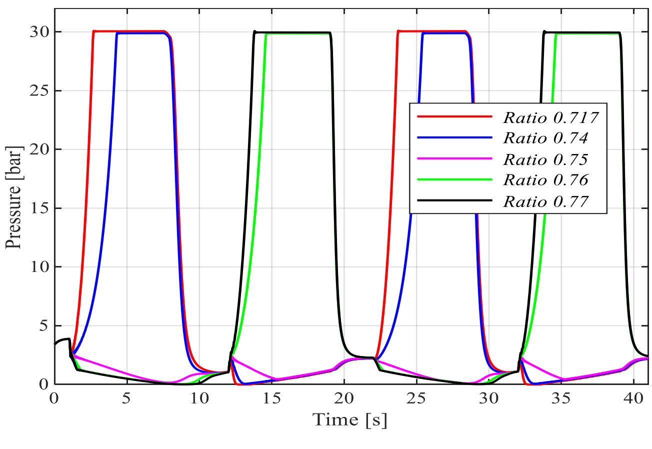

Figure 14. Pressure in the rod chamber for different displacement ratios. Cracking pressure = 30 bar.

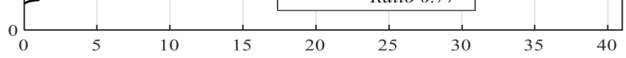

Time [s]

Figure 13. Pressure in the piston head chamber for different displacement ratios. Cracking pressure = 30 bar.

Figure 13. Pressure in the piston head chamber for different displacement ratios. Cracking pressure = 30 bar.

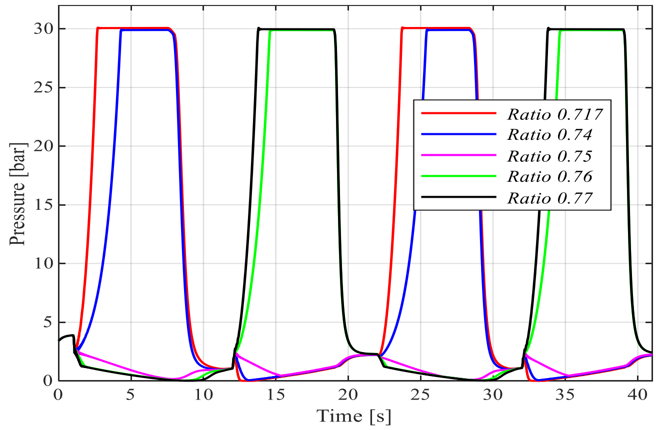

Time [s]

Figure 14. Pressure in the rod chamber for different displacement ratios. Cracking pressure = 30 bar.

Figure 14. Pressure in the rod chamber for different displacement ratios. Cracking pressure = 30 bar.

Figure 14. Pressure in the rod chamber for different displacement ratios. Cracking pressure = 30 bar.

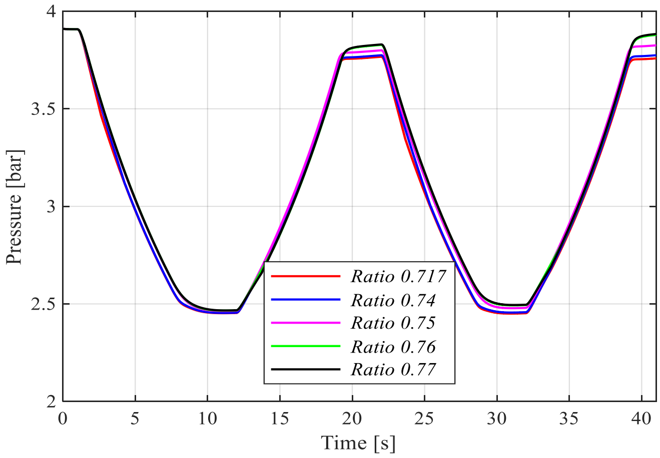

Time [s]

Figure 15. Pressure in the accumulator chamber for different ratios. Cracking pressure = 30 bar.

Figure 15. Pressure in the accumulator chamber for different ratios. Cracking pressure = 30 bar.

Figure 15. Pressure in the accumulator chamber for different ratios. Cracking pressure = 30 bar.

In order to investigate the influence of the cracking pressure of the relief valve, simulation with 5 bar was carried out under the same conditions above. Figures 16 and 17 show the pressure behavior in the chambers. The accumulator line presents similar curves as in Figure 15.

In order to investigate the influence of the cracking pressure of the relief valve, simulation with 5 bar was carried out under the same conditions above. Figure 16 and Figure 17 show the pressure behavior in the chambers. The accumulator line presents similar curves as in Figure 15.

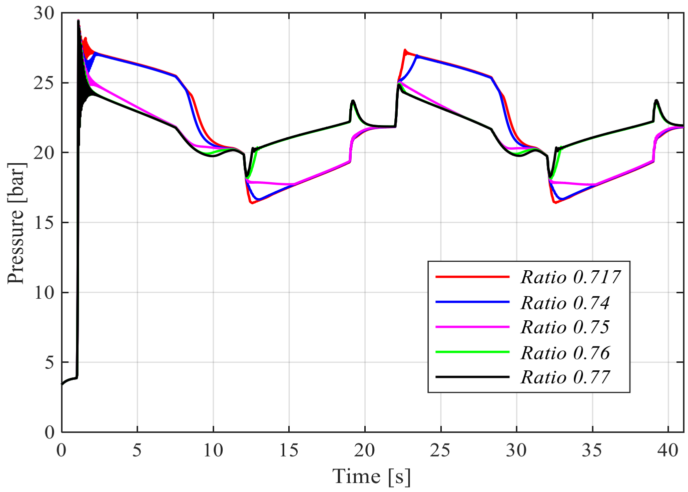

Figure 16. Pressure in the piston head chamber for different displacement ratios. Cracking pressure = 5 bar.

Figure 16. Pressure in the piston head chamber for different displacement ratios. Cracking pressure = 5 bar.

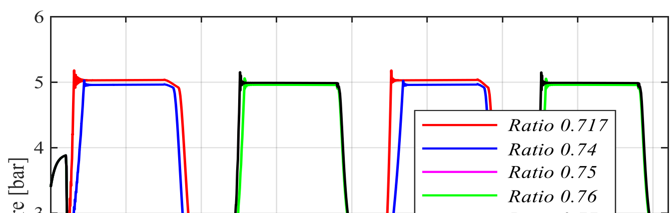

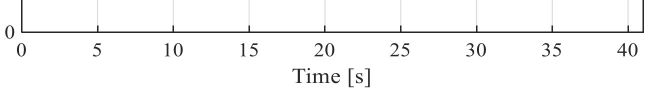

Figure 16. Pressure in the piston head chamber for different displacement ratios. Cracking pressure = 5 bar.

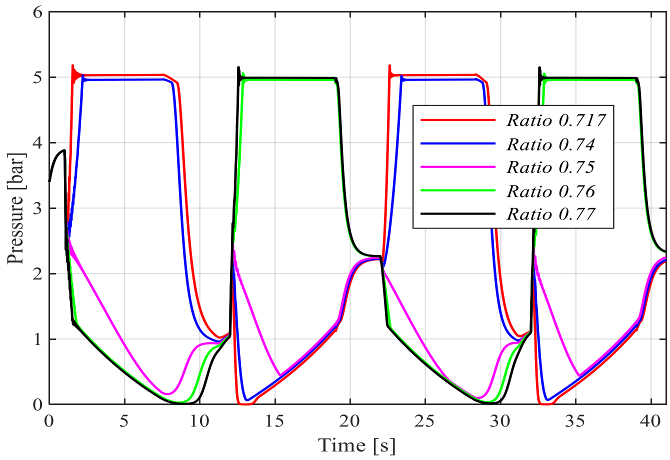

Figure 17. Pressure in the rod chamber for different displacement ratios. Cracking pressure = 5 bar.

Table 3 summarizes the overall efficiencies achieved for each displacement ratio and different system conditions. For each case performed, considering and not considering regeneration was evaluated. Ratios above 0.75 were also included to support the idea that ratios near 0.75 are in fact optimal values and higher ratios would not increase the efficiency due to the losses occurring in the pressure relief valves.

Table 3. Overall efficiency related to the volumetric displacement ratios.

	Volumetric Displacement Ratio (D_B/D_A)				
Ratio	0.717	0.74	0.75	0.76	0.77
	Efficiency (%) (CP = 30 bar)				
With regeneration	54.77	57.45	67.38	66.36	65.87
Without regeneration	34.26	35.88	42.02	42.08	42.07
	Efficiency (%) (CP = 5 bar)				
With regeneration	64.94	65.23	67.42	67.42	67.39
Without regeneration	40.57	40.77	42.05	42.15	42.15

5.3. Comparison with an Electro Hydraulic System

In order to compare the energy efficiency gained from an electro-hydrostatic actuator (EHA) with an electro hydraulic system (EHS), utilizing a cylinder controlled by a directional proportional valve with constant pressure source, both systems under the same load condition and actuator motion were analyzed. A load mass of 500 kg was assumed in order to evaluate the system performance in work conditions close to nominal operating conditions. The cylinder position (see Figure 12) was used as the reference input signal, this way it was able to evaluate the different concepts.

In the EHS model, the cylinder pressure was limited to 130 bar during an operation condition, so it was considered with a constant supply pressure of 160 bar and the efficiency of the pressure source of 75% for a variable-displacement pump (piston pump). This is the mean value for a piston pump operating between 30% and 100% of volumetric displacement at 160 bar and 1775 rev/min [14]. The directional proportional valve model was based on [15], an asymmetrical proportional valve with 2:1 orifice ratio. Figure 18 presents the pressure levels in the chambers for both actuation systems.

concepts.

In the EHS model, the cylinder pressure was limited to 130 bar during an operation condition, so it was considered with a constant supply pressure of 160 bar and the efficiency of the pressure source of 75% for a variable-displacement pump (piston pump). This is the mean value for a piston pump operating between 30% and 100% of volumetric displacement at 160 bar and 1775 rev/min [14].

The directional proportional valve model was based on [15], an asymmetrical proportional valve with 2:1 orifice ratio. Figure 18 presents the pressure levels in the chambers for both actuation systems.

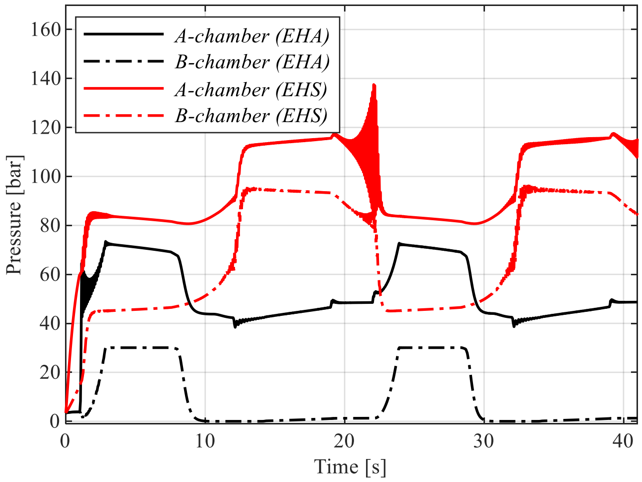

Figure 18. Pressure levels in the cylinder chambers for electro-hydrostatic actuator system (EHA) x electro hydraulic system (EHS).

Figure 18. Pressure levels in the cylinder chambers for electro-hydrostatic actuator system (EHA) x electro hydraulic system (EHS).

Table 4 presents the approximate values obtained for the condition simulated using both systems.

Table 4 presents the approximate values obtained for the condition simulated using both systems.

Table 4. Comparison of actuation systems in terms of energy consumption and efficiency.

Table 4. Comparison of actuation systems in terms of energy consumption and efficiency.

System	Max. Input Power [kW]	Input Energy [kJ]	Output Energy [kJ]	Energy Efficiency [%]
EHA (w/regeneration)	1	22.5	14.5	64.4
EHA (w/o regeneration)	1	22.5	8.7	38.7
EHS (w/prop. valve)	2.14	55	17.4	23.84

System	Max. Input Power [kW]	Input Energy [kJ]	Output Energy [KJ]	Energy Efficiency [%]
EHA (w/ regeneration)	1	22.5	14.5	64.4
EHA (w/o regeneration)	1	22.5	8.7	38.7
EHS (w/ prop. valve)	2.14	55	17.4	23.84

The results presented in Table 4 showed the amount of energy and power that can be saved ~~implementing a power-on-demand actuation system. Even adopting conservative values for pressure~~ source and prime mover efficiency, in terms of maximum input power, the EHA required only 46% of the power required by EHS, i.e., consumed. The energy consumed along the motion performed was 41% less, consequently, the overall efficiency resulted in a significant improvement.

6. Conclusions

A nonlinear dynamic model of the electro-hydrostatic actuator, including pressure and flow-dependent leakages at the pump/motors and cylinder LuGre friction, was developed and validated experimentally. Based on the simulation and experimental results, the proposed system architecture resulted in an efficiency of 38% when electrical energy regeneration is not considered, and up to 54% with energy regeneration when operating with a load mass of 40 kg.

The impact of the volumetric displacement ratio of the pump/motors is analyzed using the validated model. Since no directional valves are included in the system to balance the inflow and outflow from the differential cylinder, it should be done by the pump/motors. The results revealed that a change from ratio 0.74 to 0.75 (ideally value) on the volumetric displacement leads to a difference of 10% on the energy efficiency for a specific working cycle, load mass, and maximum rotational frequency. As a general conclusion, the design target is to select the pump/motor and cylinder with displacement ratio and area ratio, respectively, as close as possible.

Since achieving the perfect match between pump/motor and cylinder is a hard task, one option is reducing the cracking pressure of the relief valve on the rod side. Consequently, the cylinder counter-pressure is reduced, allowing the system to operate in an efficiency range near the optimal condition.

The energy performance of the proposed EHA was also compared with an EHS where the throttle losses and leakage through the proportional valve are present. The consumed energy was 46% lower to move a load of 500 kg at the same trajectory.

Therefore, besides an expected unbalance between pump/motor volumetric displacements and cylinder areas, an EHA with two pump/motors driving an asymmetrical cylinder can achieve a substantial gain considering energy consumption if compared to the conventional valve-controlled system.

Author Contributions: Conceptualization, T.M. and T.A.; validation, T.A., T.M., and V.D.N.; investigation, T.A.; resources, T.M.; writing—original draft preparation, T.A. and T.M.; writing—review and editing, T.A., T.M., and V.D.N.; supervision, T.M., V.D.N., and M.P.; project administration, T.M.; funding acquisition, T.M. and M.P. All authors have read and agreed to the published version of the manuscript.

Funding: This research was enabled by the financial support of Business Finland (Finnish Funding Agency for Innovation), project EZE, project IZIF by the Academy of Finland, CNPq—Brazilian National Council for Scientific and Technological Development (CNPq), and internal funding from Tampere University, Finland and Federal University of Santa Catarina, Brazil.

Conflicts of Interest: The authors declare no conflict of interest.

References

1. Zhang, S.; Minav, T.; Pietola, M. Improving Efficiency of Micro Excavator with Decentralized Hydraulics. In Proceedings of the BATH/ASME 2017 Symposium on Fluid Power and Motion Control, FPMC 2017, Sarasota, FL, USA, 16–19 October 2017.
2. Tasner, T.; Les, K.; Tie, V.; Lovrec, D. Energy Efficiency of Different Electro-Hydraulic Drives. In Proceedings of the 9th International Fluid Power Conference (9. IFK), Aachen, Germany, 24–26 March 2014; pp. 14–25.
3. Willkomm, J.; Wahler, M.; Weber, J. Process-adapted control to maximize dynamics of speed-and displacement-variable pumps. In Proceedings of the ASME/BATH 2014 Symposium on Fluid Power and Motion Control, Bath, UK, 10–12 September 2014.
4. Altare, G.; Vacca, A. A design solution for efficient and compact electro-hydraulic actuators. *Procedia Eng.* **2015**, *106*, 8–16. [CrossRef]
5. Gnesi, E.; Maré, J.C.; Bordet, J. Modeling of EHA Module Equipped with Fixed-Displacement Vane Pump. In Proceedings of the 13th Scandinavian International Conference on Fluid Power, Linköping, Sweden, 3–5 June 2013; pp. 141–152.
6. Padovani, D.; Ketelsen, S.; Hagen, D.; Schmidt, L. A self-contained electro-hydraulic cylinder with passive load-holding capability. *Energies* **2019**, *12*, 292. [CrossRef]
7. Pietrzyk, T.; Roth, D.; Schmitz, K.; Jacobs, G. Design study of a high speed power unit for electro hydraulic actuators (EHA) in mobile applications. In Proceedings of the 11th International Fluid Power Conference, Aachen, Germany, 19–21 March 2018; pp. 233–245.
8. Quan, Z.; Quan, L.; Zhang, J. Review of Energy Efficient Direct Pump Controlled Cylinder Electro-Hydraulic Technology. *Renew. Sustain. Energy Rev.* **2014**, *35*, 336–346. [CrossRef]
9. Schneider, M.; Koch, O.; Weber, J.; Bach, M.; Jacobs, G. Green Wheel Loader–Development of an energy efficient drive and control system. In Proceedings of the 9th International Fluid Power Conference, Aachen, Germany, 24–26 March 2014; pp. 24–26.
10. Wei, S.G.; Zhao, S.D.; Zheng, J.M.; Zhang, Y. Self-tuning dead-zone compensation fuzzy logic controller for a switched-reluctance-motor direct-drive hydraulic press. *Proc. Inst. Mech. Eng. Part I J. Syst. Control Eng.* **2009**, *223*, 647–656. [CrossRef]
11. Wang, L.; Book, W.J.; Huggins, J.D. A hydraulic circuit for single rod cylinders. *J. Dyn. Syst. Meas. Contr.* **2012**, *134*, 011019. [CrossRef]
12. Järf, A. Flow Compensation Using Hydraulic Accumulator in Direct Driven Hydraulic Differential Cylinder Application and Effects on Energy Efficiency. Master's Thesis, Aalto University, Espoo, Finland, 2016.
13. Ketelsen, S.; Padovani, D.; Andersen, T.O.; Ebbesen, M.K.; Schmidt, L. Classification and Review of Pump-Controlled Differential Cylinder Drives. *Energies* **2019**, *12*, 293. [CrossRef]

14. Bravo, R.R.S. Sistema hidráulico-pneumático de frenagem regenerativa e hibridização de veículos comerciais. Ph.D. Thesis, Federal University of Santa Catarina, Florianópolis, Brazil, 2017.
15. Destro, M.C.; De Negri, V.J. Method for combining valves with symmetric and asymmetric cylinders for hydraulic systems. *Int. J. Fluid Power* **2018**, *19*, 126–139. [CrossRef]